


Enzyme-assisted mechanical production of cellulose nanofibrils: thermal stability

Kun Zhang · Yuehua Zhang · Depeng Yan · Chenyuan Zhang · Shuangxi Nie 

Received: 7 May 2018 / Accepted: 3 July 2018 / Published online: 5 July 2018
© Springer Nature B.V. 2018

Abstract The influence of enzymatic treatment on the thermal stability of cellulose nanofibrils (CNFs) was investigated. The unbleached bagasse pulp was treated with different dosages of xylanase, and samples were taken at different grinding stages. The produced CNF were characterized by Malvern Zetasizer, TEM, ATR-FTIR and XRD, and the thermal stability of the CNF was evaluated using TGA. The mechanism of enzymatic treatment on the thermal stability of CNF was proposed. The results indicated that all the diameters of produced CNF were

< 100 nm. The CNF produced from original pulp has higher thermal stability than those from enzymatic-treated pulp, and the thermal stability of CNF was decreased with the increase of enzyme dosage. The practical application of CNF was actually limited by the reduction of pyrolysis sites, so the proper retention of hemicellulose and lignin in the process of preparing CNF contributes to the improvement of the thermal stability.

Kun Zhang and Yuehua Zhang have contributed equally to this work.

K. Zhang · Y. Zhang · D. Yan · C. Zhang · S. Nie (✉)
College of Light Industry and Food Engineering, Guangxi University, Nanning 530004, People's Republic of China
e-mail: nieshuangxi@gxu.edu.cn

K. Zhang
e-mail: zhangkun011@yeah.net

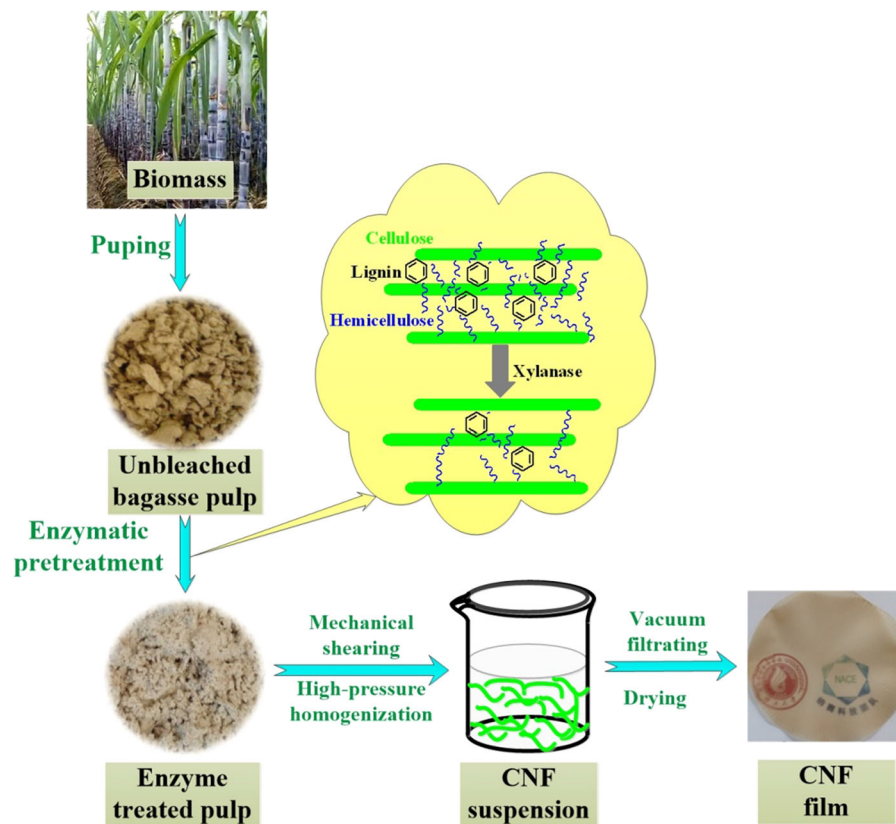
Y. Zhang
e-mail: 18364237652@163.com

D. Yan
e-mail: 798791084@qq.com

C. Zhang
e-mail: 644659411@qq.com

K. Zhang · Y. Zhang · D. Yan · C. Zhang · S. Nie
Guangxi Key Laboratory of Clean Pulp & Papermaking and Pollution Control, Nanning 530004, People's Republic of China

Graphical abstract



Keywords Cellulose nanofibrils · Enzymatic treatment · Xylanase · Thermal stability

Introduction

With the emergence of global environmental changes and resource shortages, there is a growing interest in sustainable and environmentally friendly materials (Nie et al. 2014; Yao et al. 2017). Trees are sustainable and renewable materials, and lignocellulosic biomass has the advantages of good biocompatibility, non-toxicity and biodegradability compared to synthetic polymers (Peng et al. 2011; Song et al. 2016; Xu et al. 2017). In recent years, the development of new materials from cellulose nanofibrils (CNF) with lignocellulosic biomass as the raw material is significant (Liu et al. 2017b; Yao et al. 2015). CNF has been found to have unique optical properties, mechanical properties, thermal properties, refractive index,

dielectric constant, and barrier properties. CNF can be used to prepare cellulose-based electronic flexible transistors, organic light-emitting diodes (OLEDs), printed and radio frequency identification (RFID) equipment, high-performance speakers, lightweight paper actuators, writeable touch screens and other green electronic products (Zhu et al. 2016).

The thermal stability of CNF is directly related to the quality of cellulose-based green electronic products. There are many factors that affect the thermal stability of CNF, such as plant fiber raw material components (hemicellulose, lignin, etc.) as well as the grinding, drying and post-modification processes (Li et al. 2018). CNF has a large specific surface area and a large endothermic area, so the thermal stability of CNF was generally lower than that of the original fibers (Jiang and Hsieh 2013). Lu and Hsieh measured the initial decomposition temperature of CNF prepared by sulfuric acid hydrolysis at 150 °C, and the maximum decomposition rate was < 300 °C. Due to the introduction of sulfonic acid groups, the thermal

stability of CNF is seriously reduced, because the thermal decomposition of cellulose has a catalytic effect (Lu and Hsieh 2010). To prove this point, Martínez-Sanz neutralized the CNF obtained by hydrolyzing sulfuric acid with NaOH, so the surface of the introduced sulfonic acid groups was removed; consequently, the thermal stability of CNF after neutralization was improved (Martínez-Sanz et al. 2011). A carboxyl group introduced in the CNF also decreased the thermal stability, and Jiang prepared CNF using TEMPO oxidized rice straw. The initial decomposition temperature was approximately 210 °C, and the maximum decomposition rate was 265 °C (Jiang and Hsieh 2013). Nair and Yan studied the effect of lignin on the thermal stability of CNF and found that when the content of lignin in CNF was 21 and 5%, the degradation temperatures of CNF were 306 and 278 °C, respectively. The maximum degradation rates were 390 and 319 °C, respectively. The thermal stability of CNF was significantly improved due to the presence of lignin (Nair and Yan 2015).

Environmentally friendly enzyme-assisted preparation of micro-nanofiber technology is a reliable lignocellulosic biomass high value green utilization technology (Lin et al. 2018; Long et al. 2017; Nie et al. 2015). Arola et al. pretreated the fibers with xylanase, and the rheological properties, morphological characteristics and properties of CNF paper films were studied. It was found that the removal of xylan could enhance the formation of the fibril network and stabilize the fibrils, thereby preventing CNF flocculation (Arola et al. 2013). Dhandapani and Sharma used mechanical methods combined with biological enzymes to treat cannabis fibers (cellulose content of approximately 78%). CNF was successfully prepared, and the average diameter was 29.5 nm (Dhandapani and Sharma 2014). Henriksson et al. treated wood pulp with endoglucanase or acid hydrolysis and mechanical shearing, and microfibrillated cellulose was isolated from the fibroblast cell wall. The CNF was observed using atomic force microscopy (AFM), and it was found that enzyme treatment can promote the separation of CNF and exhibits a higher than average molar mass as well as a higher aspect ratio compared to CNF produced by acid pretreatment (Henriksson et al. 2007).

In this paper, the effects of xylanase pretreatment on the thermal stability of CNF were studied. CNF was obtained by pretreatment of unbleached bagasse pulp

using xylanase, combined with ultra-fine grinding and high pressure homogenization. The CNF was characterized by TEM, ATR-FTIR and Zeta potential meter. Thermal stability of CNF was characterized by XRD and thermogravimetric analysis. The research results provide a theoretical basis for the pyrolysis mechanism and high utilization of CNF, which had a profound effect and important strategic significance on development of new nano-materials and related discipline collaborative innovation.

Materials and methods

Chemicals and raw materials

Unbleached bagasse pulp was produced in the Guangxi Yongkai Paper Mill. The xylanase model is Novozyme X2753, and the enzyme activity was 2980 IU/g (Sigma-Aldrich). Sealed bags, citric acid, and disodium hydrogen phosphate were from Guangxi Nanning Boyu Limited. The water used in the experiment was deionized, and the chemicals were of analytical grade.

Sample preparation

Xylanase pretreatment

A total of 200 g dry and unbleached bagasse wood pulp was sealed in a pulp bag. Pre-configured citric acid-disodium hydrogen phosphate buffer solution (pH 6.0) was added, and 0 IU/g (control), 5, 10 and 30 IU/g xylanase were added. When fully and evenly mixed, the pulp concentration remained at approximately 8%. The samples were placed in a constant temperature water bath for enzyme pretreatment at a temperature of 50 °C for 2 h. Every 10–15 min, the samples were constantly stirred to achieve the enzyme full effect. When the reaction was over, the enzyme was inactivated at 100 °C for roughly 30 min, and the sample was washed several times until it was neutral after approximately 12 h in the refrigerator storage with a good water balance.

CNF preparation

The xylanase pretreated pulp was distilled at a concentration of 2% (w/w) and disintegrated for

30 min. Then, the Super grinding mill (MKZA10-15J, Japan) was used for grinding, controlling the gap between the two discs in the 0 points below the gap of 4 grid grinding. All samples were ground for 10 passes. After grinding, the samples were homogenized by passing through a Microfluidizer high-pressure homogenizer (M-110EH-30, USA) 20 times to obtain CNF. The diameter of each chamber in the chamber pair were 200 and 87 μm , and the homogenization pressure was controlled at 20,000 psi (Nie et al. 2018). The prepared CNFs were diluted to 1% (w/w) and stored in the refrigerator. 5 and 30 IU/g xylanase pretreated pulp were also sampled before grinding with 1 pass, 5 passes, 10 passes.

Freeze-drying

The prepared CNFs were placed on a circular watch glass with a diameter of 10 cm and pre-frozen for 8 h in an ultra-low temperature refrigerator at $-80\text{ }^{\circ}\text{C}$. Then, the pre-frozen samples were freeze-dried for 36 h via a freeze-drying system (ALPHAL-4 LD PLUS, CHRIST, German), and the dried samples were transferred to a drying basin for use.

Preparation of the CNF film

The prepared CNFs were diluted to a concentration of 1%, and the CNFs with an absolute dry weight of 0.24 g were placed in a 250 ml Erlenmeyer flask. Next, 250 ml of deionized water was added and fully stirred for 2 h; the sample was vacuum filtered with a 0.22 μm polytetrafluoroethylene film, and then dried in a drying basin at $50\text{ }^{\circ}\text{C}$ for 12 h.

Analysis methods

Zeta potential and fiber dimensions

Zeta potential and fiber dimensions of the produced CNF were analysed by Malvern Zetasizer (Nano-ZS90X, UK). The Malvern Zetasizer was turned on and waiting for 30 min until a steady state is achieved. The Zeta potential measurement model was selected for the analysis of Zeta potential and fiber dimensions after the instrument self-test. 1 ml CNF suspension were taken and put into the sample pool, and the measuring can be started.

Transmission electron microscopy (TEM)

The control, 5, 10 and 30 IU/g xylanase treated CNFs were distilled at a concentration of 0.01% (w/w). 2 drops of the CNF suspension were applied on holey carbon copper grid, and the grid were naturally dried at room temperature for 12 h. The samples were then dyed by uranyl acetate, and placed for 10–30 min in dark. TEM (Hitachi HT7700, Japan) was performed using an acceleration voltage of 100 kV and electric current of 10 μA .

ATR-FTIR spectra

Functional groups change of the CNF were analyzed by ATR-FTIR spectra (SENSOR II, Brook technology, Germany). Blank determination was carried out before the analysis of the samples, and the CNF were then flatted on the platform. The measurement started when the detector lamp exactly pressed to the films, and the spectrum for each sample was recorded in the region of $4000\text{--}800\text{ cm}^{-1}$ at a resolution of 4 cm^{-1} (Nie et al. 2018).

Thermogravimetric (TGA)

The freeze-dried samples were subjected to thermogravimetric analysis using a synchronous thermal analyzer (STA 449F5, NETZSCH, Germany). All samples analyses were conducted under a nitrogen atmosphere, and the samples were filled with alumina crucibles. Samples weighing approximately 10 mg were controlled by heating at a rate of 2, 5 and $10\text{ }^{\circ}\text{C}/\text{min}$ from 100 to $600\text{ }^{\circ}\text{C}$. Each sample was tested in triplicate.

X-ray diffraction (XRD)

The dried CNF film was subjected to crystallinity analysis using a high-resolution X-ray diffractometer (MINIFLEX600, Japan). The samples were cut into $2 * 2\text{ cm}$ squares with scissors and then attached to the glass sample plate with clear tape. To ensure that the film was flat on the sample plate, the same sample rack position and sample rack were controlled. The scanning angle 2θ was in steps of 0.02° at 2.5 s per step from 5° to 60° , and the CNF crystallinity index (CI) was calculated as follows (Segal et al. 1959):

$$CI = 100 \times \frac{I_{200} - I_{am}}{I_{200}}$$

where I_{200} is the diffraction intensity at $2\theta \approx 22.5^\circ$, which represents a crystalline region; I_{am} is the diffraction intensity of $2\theta = 18^\circ$, indicating an amorphous region.

Results and discussion

Characteristics of the produced cellulose nanofibrils

The charge, dimension and morphology of the CNF can have high influence not only on the thermal stability and crystallinity of the final product but also on the cost of the process. The particle charge and dimension scale were analyzed by Malvern Zetasizer. Table 1 shows the average particle diameter, Zeta potential, carboxyl group content and hemicellulose content of the CNF suspension with different dosage of xylanase treatment. It can be seen that, the Zeta potential (negative charges) and carboxyl group content increased as the amount of xylanase increased after the same grinding and homogenization number. The Zeta potential can reach to -42.7 mV, and CNF average particle diameter of 48.49 nm when the dosage of xylanase was 30 IU/g. This because that the fibers become looser after xylanase treatment, and more carboxyl groups are exposed on fiber in subsequent mechanical treatment. Zeta potential is an important index to characterize the stability of the CNF suspension. The negative charge on the surface of CNF particles increase when the absolute value of the Zeta potential increase. The repulsive force between fibers increase after xylanase treatment, which will cause the fibers to separate from each other (Khouri 2010). The surface morphology of the

produced CNF with different dosage of xylanase treatment were shown in Fig. 1. It can be seen that, the TEM shows long, well-defined and distinct CNF, and all the diameters of produced CNF were < 100 nm, which was similar to the results of Malvern Zetasizer (Table 1).

ATR-FTIR analysis of the cellulose nanofibrils

The ATR-FTIR can be used to analyze changes of the chemical groups on the surface of the produced CNF. The ATR-FTIR spectra of the control, 5, 10 and 30 IU/g xylanase treated CNFs films shown in Fig. 2. It can be seen that, 3351 cm^{-1} associated to the $-\text{OH}$ stretching frequencies of cellulose, and it was higher than the control after xylanase treatment. It means that xylanase treatment could obviously increase the content of $-\text{OH}$ in CNF. 1731 cm^{-1} associated to the carboxyl group (Nie et al. 2018), and it was higher than the control after xylanase treatment, meaning that more hydrophilic carboxyl groups were exposed to the fiber surface after enzymatic treatment and refining. The presence of carboxyl groups will affect the thermal stability of CNF, because that it will be degraded at lower temperatures (Meng et al. 2016). The bands at 1105, 1130, 1145, 1259, 1270, 1615 and 1652 cm^{-1} associated to the $-\text{CH}$, $-\text{OH}$ and $-\text{CH}_2$ bending frequencies, indicated that a great number of lignin was contained in the pulp (Nie et al. 2015). The lignin-carbohydrate complex (LCC) was destroyed after xylanase treatment, and more lignin is released and redeposited on the fiber surface. Nair and Yan studied the effect of lignin on the thermal stability of CNF. By comparing the effects of high and low lignin content on the thermal stability of CNF, it was found that residual lignin had a significant effect on the thermal stability of CNF; the higher the content of CNF, the higher was the thermal stability of CNF (Nair and Yan 2015). Gordobil et al. extracted the xylan-rich

Table 1 The particle diameter, Zeta potential and carboxyl group content of CNF

Sample	Particle diameter (nm)	Zeta potential (mV)	Carboxyl group content (mmol/g) (Nie et al. 2018)	Hemicellulose content (%)
Control	61.68	-22.7	0.14	24.8
5 IU/g xylanase	60.61	-33.5	0.15	20.7
10 IU/g xylanase	50.03	-38.3	0.16	16.9
30 IU/g xylanase	48.49	-41.0	0.18	14.1

Fig. 1 TEM images of the produced CNF with different dosage of xylanase treatment. **a** Control; **b** 5 IU/g xylanase; **c** 10 IU/g xylanase; **d** 30 IU/g xylanase

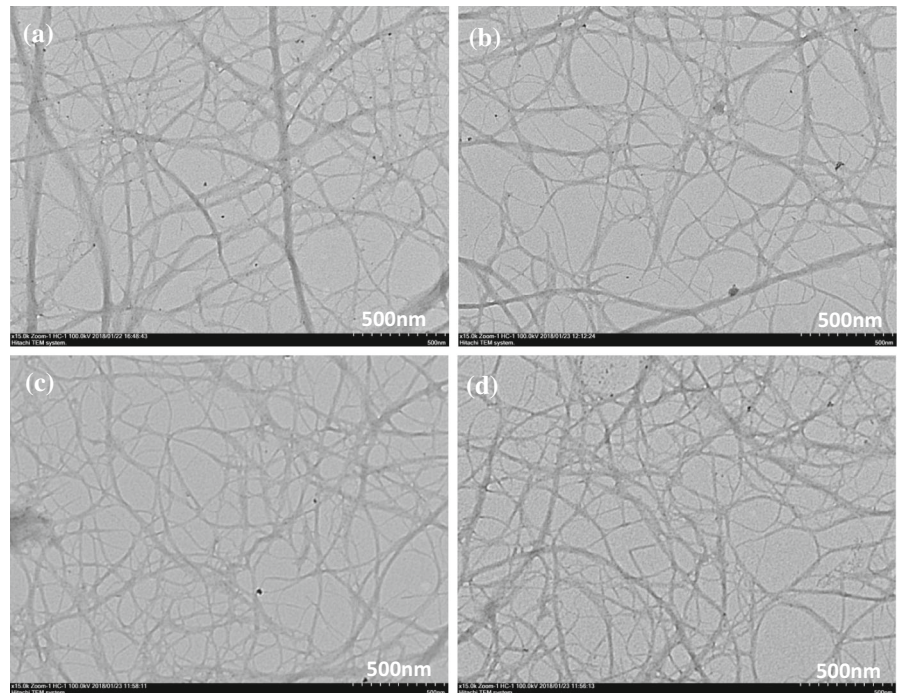
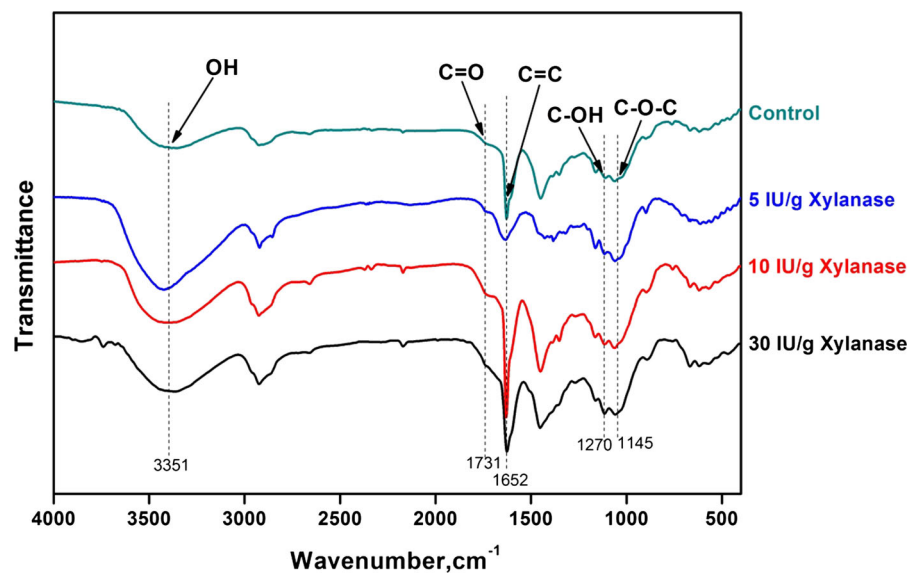


Fig. 2 ATR-FTIR spectra of the produced CNF with different dosage of xylanase treatment



hemicellulose from corncob, and the hemicellulose was composited with cellulose after acetylation. They found that the thermal stability and mechanical properties improved significantly with the existence of hemicellulose (Gordobil et al. 2014). The practical

application of CNF was actually limited by the reduction of pyrolysis sites, so the proper retention of hemicellulose and lignin in the process of preparing CNF contributes to the improvement of the thermal stability.

Thermal stability of the cellulose nanofibrils

In recent years, CNF applications have been more widely used, and CNFs are expected to replace some plastic and glass substrates. However, CNF will also be degraded at high temperatures. At present, scholars have studied the thermal stability of cellulose (Azubuike et al. 2011; Gedler et al. 2012; Jacquet et al. 2011; Liu et al. 2017a). These studies allowed us to better understand the pyrolysis mechanism of cellulose and provide a reference for future composites that use CNF to make better heat-resistant properties. The thermal decomposition of cellulose mainly produces flammable volatile matter and is released by dehydration, hydrolysis, oxidation, decarboxylation and transglycosylation (Chen et al. 2013). In this study, samples were subjected to thermogravimetric analysis under the protection of a nitrogen atmosphere, and the temperature was raised from 100 to 400 °C.

The TGA curve of CNF at a heating rate of 10 °C/min is shown in Fig. 3. Depending on the weight percentage of the sample with temperature, the TGA curve for each sample could be divided into three regions. As shown in Fig. 3a, since the moisture content of the fiber sample is vaporized, 25–220 °C was region I, which was defined as the initial mass loss stage. The sample had a slight mass loss in this region, typically < 8%, and no thermal degradation occurred. Figure 3b shows the detailed TGA curve of the sample in region I. It can be seen that the mass loss rate of the

sample is always in the stationary stage when heated from 130 to 220 °C. Between the CNF samples prepared after the enzyme treatment and the control group, the same TGA curve trend was typically observed. As the temperature increased, the moisture content of the CNF sample was first eliminated. Then, all of the residual moisture was evaporated, thereby achieving a stable period of constant mass. The evaporation rate of each sample appears to be consistent, and the temperature difference in the stationary period was not significant. At the steady temperature stage, the mass loss rates of the control samples and those treated with 5, 10 and 30 IU/g xylanase were 7.4 ± 0.1 , 7.7 ± 0.5 , 4.9 ± 0.3 and $3.9 \pm 0.3\%$, respectively (Table 2).

The region of the sample TGA curve was defined as the main mass loss stage. As shown in Fig. 3b, 220 °C (end temperature of region I) was defined as the initial temperature of thermal degradation. The TGA curve of the samples began to deviate from the steady region from roughly 220 °C. Kilzer and Broido suggested that the dehydration of cellulose to produce “dehydrated cellulose” had an endothermic temperature of approximately 200–280 °C, and the depolymerized cellulose competed with dehydration from 280 to 340 °C, resulting in the formation of volatiles (Long et al. 2017). As shown in Table 2, the residual mass and temperature of the control sample at the end of region II were 20.48% and 380 °C, respectively, and the residual mass of the CNF sample after enzyme treatment was above 25% at the end of region II. This

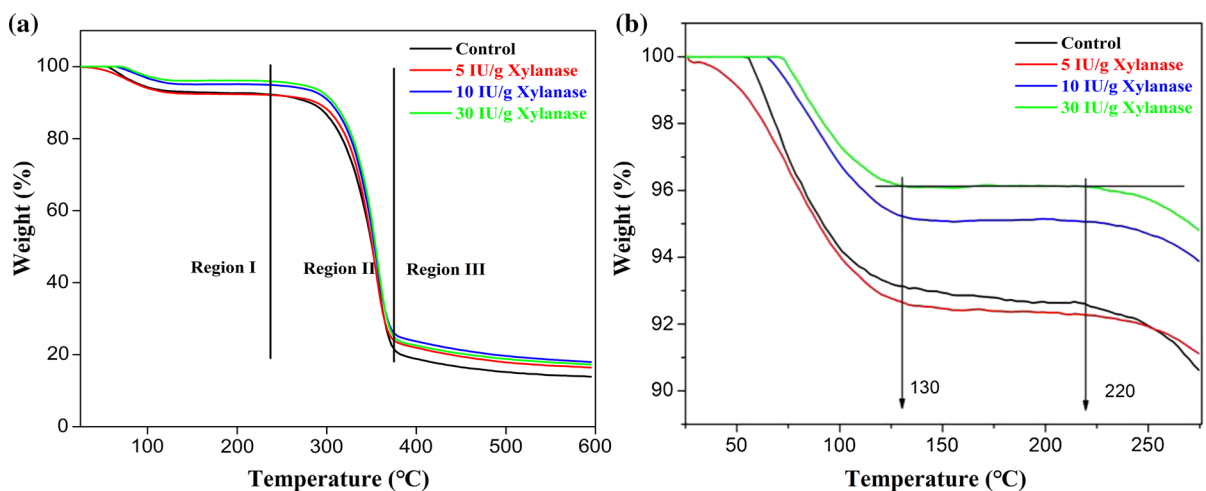


Fig. 3 TGA curves of the xylanase pretreated cellulose nanofibrils at a heating rate of 10 °C/min. **a** from 25 to 600 °C, **b** from 25 to 276 °C in detail

Table 2 Thermal stability of the cellulose nanofibrils

Sample	Region I		Region II		Region III
	Temperature (°C)	Moisture residue (wt %)	Temperature (°C)	Mass residue (wt %)	Mass residue (wt %)
Control	220	7.4 ± 0.1	380	20.5 ± 0.1	13.9 ± 0.2
5 IU/g xylanase	225	7.7 ± 0.5	370	25.6 ± 0.8	16.4 ± 0.3
10 IU/g xylanase	225	4.9 ± 0.3	370	28.3 ± 0.4	17.9 ± 0.7
30 IU/g xylanase	225	3.9 ± 0.3	370	27.6 ± 0.2	17.3 ± 0.1

demonstrated that the thermal degradation of the sample in region II was reduced by enzyme treatment. After region II, the mass loss rate of the cellulose sample was reduced (Fig. 3a). The TGA curve from this point to the final test temperature of 600 °C was defined as region III, and this stage was the graphitization stage of cellulose. The residues of the cellulose structure were aromatic and gradually formed a graphite structure (Shafizadeh 1982). In region III, when the temperature exceeded 500 °C, the cellulose decomposed to produce various low molecular weight products, including low-molecular-weight organic matter, CO, CO₂ and H₂O (Peng et al. 2013). At the final test temperature of 600 °C, the final residues of the control sample and CNF samples treated with 5, 10 and 30 IU/g xylanase were 13.9 ± 0.2, 16.4 ± 0.3, 17.9 ± 0.7 and 17.3 ± 0.1%, respectively (Table 2). It could be seen that the residue of the control sample was the lowest, and the mass of the CNF obtained by the enzymatic treatment were increased after high temperature degradation. These results may occur because the enzyme removed part of the hemicellulose and lignin, and the cellulose more easily formed an aromatic ring, forming a graphite structure. The sample underwent a water evaporation process at higher temperatures, and the surface of the nanofibers became compact to form a graphite structure, thereby reducing the thermal degradation of the fibrils (Meng et al. 2016).

In the nitrogen atmosphere, the CNF samples prepared after xylanase treatment and the comparative samples were subjected to thermogravimetric analysis (TGA), and the heating rates were controlled at 2, 5 and 10 °C/min. Figure 4 shows the TGA curves for each sample at heating rates of 2, 5 and 10 °C/min. In order to better compare the thermal behavior of each sample, the weight loss due to moisture in the sample during the experiment was not considered (0–5% from

30 to 100 °C). Therefore, the starting point of the TGA and DTG curves for each sample is set to 100 °C. The temperatures at which the sample weight loss was 3, 5, and 10% and the peaks of the DTG curve were recorded as T_{3%}, T_{5%}, T_{10%} and T_d, respectively. All samples were controlled from 100 to 600 °C to observe their thermal degradation. The effects of different heating rates on the thermal stability of four different CNFs are shown in Table 3.

It can be seen from Fig. 4 and Table 3 that heating rate increase, T_{3%}, T_{5%}, T_{10%} and T_d all showed an increasing trend. There was no significant difference in the maximum thermal decomposition temperature of the four samples when the heating rate was 2 and 5 °C/min. The thermal stability of the control sample was significantly higher than that of the three samples treated with xylanase when the heating rate was 10 °C/min. The reason is that cellulose decomposes relatively easily at high heating rates and forms more volatiles in a short time (Shen and Gu 2009). In general, the higher the heating rate, the smaller is the effect of mass transfer control. The holes in the DSC crucible greatly influenced the mass transfer control, resulting in a change in the amount of DSC per unit time (Milosavljevic et al. 1996). The maximum degradation temperatures of the control sample and the xylanase-treated samples with 5, 10 and 30 IU/g were 354, 342, 339 and 335 °C, respectively, when the heating rate was 10 °C/min. CNF obtained after xylanase treatment contain a higher carboxyl content (Nie et al. 2018), and the carboxyl group affects the thermal stability of CNF (Meng et al. 2014). The presence of carboxyl groups promoted the decarboxylation reaction during the thermal degradation of CNF (Stamm 1956), which caused the cellulose to be pyrolyzed into small molecule products (Zhu et al. 2012), thereby reducing the cellulose stability. By selectively oxidizing the primary hydroxyl groups at

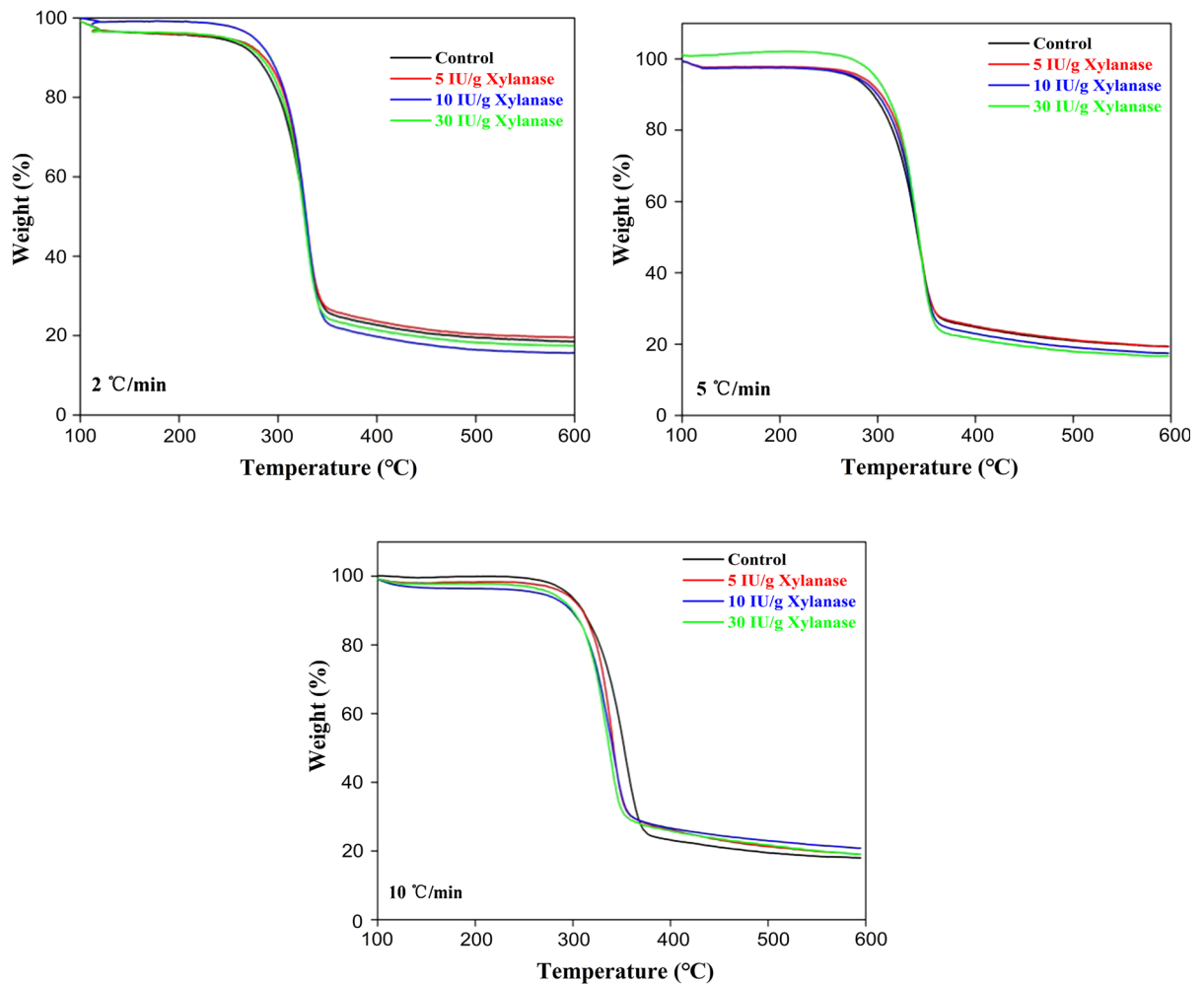


Fig. 4 TGA analysis of the cellulose nanofibrils heated at 2, 5 and 10 °C/min

Table 3 TG data of the CNF, heated at 2, 5 and 10 °C/min

Sample	2 °C/min				5 °C/min				10 °C/min			
	T _{3%}	T _{5%}	T _{10%}	T _d	T _{3%}	T _{5%}	T _{10%}	T _d	T _{3%}	T _{5%}	T _{10%}	T _d
Control	118.5	236	278	329	241	274	295	343	284	295	310	354
5 IU/g xylanase	119	246	286	328	258	283	304	343	275	291	310	342
10 IU/g xylanase	232	275	292	328	242	278	300	343	251	266	300	339
30 IU/g xylanase	119	246	283	328	271	298	309	343	276	278	300	335

the C6 position of the cellulose to carboxyl groups, Kumar and Yang (2002) found that the thermal stability of the modified cellulose deteriorated and that T_d decreased with increasing carboxyl content.

Thermal stability for samples at different stages of fibrillation

Thermal stability is a very important parameter for CNF as a composite material. Two important

temperature characteristics, T_{onset} and T_d , could be obtained by analyzing the TGA mass loss curve and its derivative curve with temperature. T_{onset} was defined as the temperature at which the sample mass loss begins to change significantly and could be obtained by a tangent method (Fig. 5). T_d was the maximum value of the weight curve derivative, and the sample was most rapidly degraded at this temperature (Nair and Yan 2015; Valkenburg et al. 2005). Table 4 shows the particle diameter, T_{onset} and T_d values for the xylanase-pretreated fibers at different stages of fibrillation. As seen from Table 4, the T_{onset} values of the fibers treated with 5 and 30 IU/g xylanase were 302 and 299 °C, respectively, and the T_d values were 359 and 364 °C, respectively. When the number of mechanical grinds was different, the T_{onset} and T_d values of the fiber samples treated by the xylanase showed a decreasing trend with the increasing number of grinding channels indicating that the fiber size will

affect its thermal stability. Therefore, thermal stability of the small size CNF is lower than the bigger one because the small size CNF have a much larger specific surface area and are more likely to be exposed during heating. Thus, the pyrolysis rate was accelerated and the corresponding thermal stability was ultimately reduced (Quiévy et al. 2010).

The cellulose crystallinity was also affected by the thermal stability, and the X-ray diffraction spectra of the fibers of different grinding channels after enzyme treatment are shown in Fig. 6. The X-ray display of the peak diffraction pattern was composed of several different crystal face composite peaks, and the main diffraction peaks $2\theta = 14.8^\circ$, 16.3° , 22.5° , and 34.5° corresponded to the Miller indices, respectively, at -110 , 110 , 200 and 004 (French 2014; Nishiyama et al. 2003). The crystallinity index of the fiber could be calculated from the height ratio between the crystal intensities (Segal et al. 1959). The crystallinity of the

Fig. 5 TGA and DTG for the xylanase pretreated cellulose nanofibrils at different stages of fibrillation

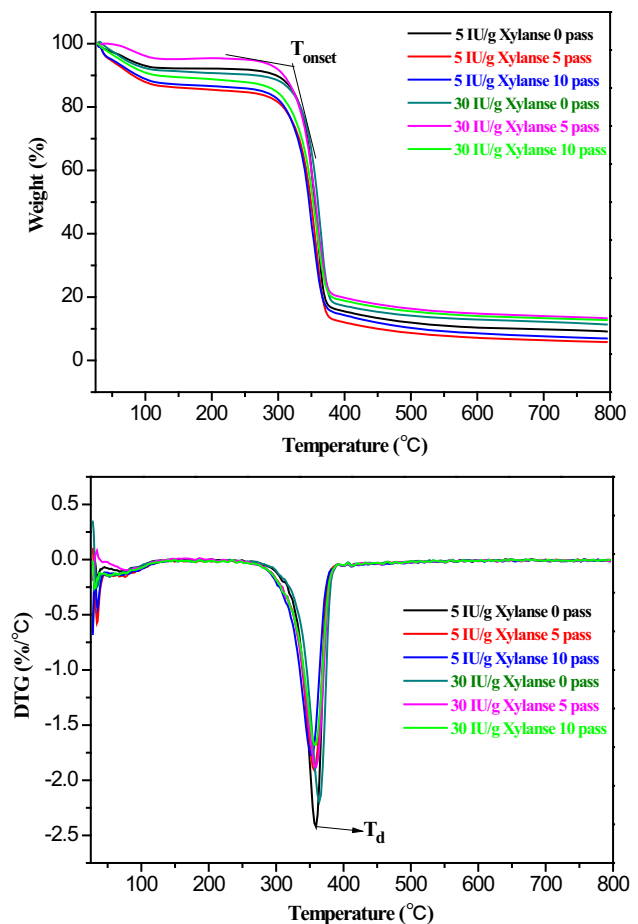
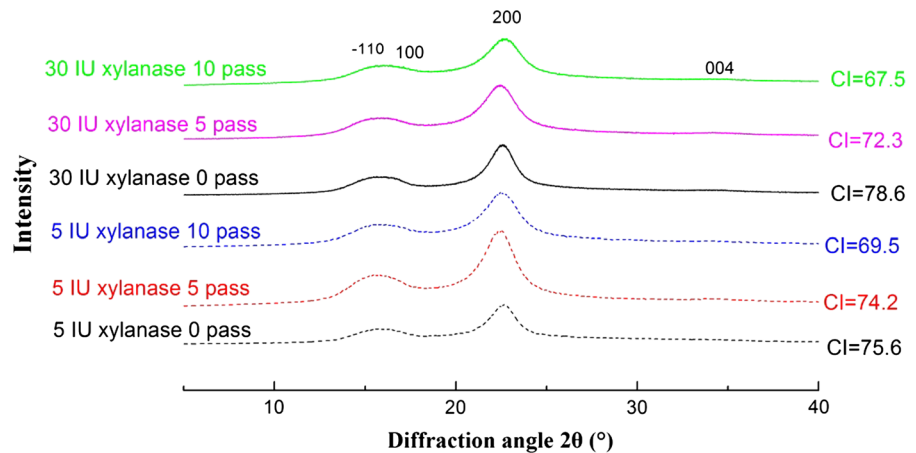


Table 4 Particle diameter, T_{onset} and T_d values for the xylanase pretreatment of fibers at different stages of fibrillation

Sample	Particle diameter (nm)	T_{onset} (°C)	T_d (°C)
5 IU/g xylanase 0 pass	113.2	302	359
5 IU/g xylanase 5 pass	88.3	294	356
5 IU/g xylanase 10 pass	60.6	287	354
30 IU/g xylanase 0 pass	90.5	299	364
30 IU/g xylanase 5 pass	75.1	290	359
30 IU/g xylanase 10 pass	48.5	287	356

Fig. 6 XRD profiles from films of cellulosic samples

fiber treated with 30 IU/g xylanase prior to grinding was 78.6, which was higher than that of the 5 IU/g xylanase treated fiber sample (75.6). These results might occur because when the amount of xylanase was greater, the hemicellulose and lignin in the fiber were degraded and dissolved (Gordobil et al. 2014). Hydrolyzed hemicellulose was mainly in the amorphous area, so the proportion of the corresponding crystallization region after enzyme treatment would rise, and the crystallinity index would also rise. As the number of grinding passes increased, the crystalline area of the cellulose was destroyed and the length of the cellulose chain was shortened, resulting in a smaller crystal area and thereby reducing the crystallinity of the sample (Nair and Yan 2015). However, the increased carboxyl groups and decreased fiber size are considered to decrease the thermal stability, while, the increase of crystallinity is normally considered to increase the thermal stability. In fact, the fiber size and hemicellulose content have the main effect on the thermal stability of CNF than the effect of crystallinity. The thermal stability of the cellulose samples was increased by a relatively low degree of crystallinity and a relatively large size. It could be seen

that, in terms of thermal stability, the cellulose samples without grinding had higher stability values than those after grinding.

Conclusions

Xylanase-aided mechanical production of CNF from unbleached bagasse pulp was assessed to evaluate the effect of enzymatic treatment on the thermal stability of CNF. It appeared that proper retention of hemicellulose and lignin in CNF is helpful for improving the thermal stability of CNF. This work opens the door for CNF production from unbleached pulp and will simplify the complicated purification process. In addition, high haze CNF with a small amount of hemicellulose are a potential substrate for flexible solar cells. The hemicellulose particles will increase light blockage and thus improve the energy storage efficiency of solar cells.

Acknowledgments This project was supported by the National Natural Science Foundation of China (31760192), the Scientific Research Foundation of Guangxi University

(XGZ160166), and the Guangxi Natural Science Foundation of China (2016GXNSFBA380234).

References

- Arola S, Malho JM, Laaksonen P, Lille M, Linder MB (2013) The role of hemicellulose in nanofibrillated cellulose networks. *Soft Matter* 9:1319–1326. <https://doi.org/10.1039/c2sm26932e>
- Azubuiké CP, Rodríguez H, Okhamafe AO, Rogers RD (2011) Physicochemical properties of maize cob cellulose powders reconstituted from ionic liquid solution. *Cellulose* 19:425–433. <https://doi.org/10.1007/s10570-011-9631-y>
- Chen Y, Tshabalala MA, Gao J, Stark NM, Fan Y (2013) Color and surface chemistry changes of extracted wood flour after heating at 120°C. *Wood Sci Technol* 48:137–150. <https://doi.org/10.1007/s00226-013-0582-3>
- Dhandapani R, Sharma S (2014) Environmentally benign pretreatments for producing microfibrillated cellulose fibers from hemp. *Lightweight materials from biopolymers and biofibers*. ACS symposium series, vol 1175. American Chemical Society, Washington. <https://doi.org/10.1021/bk-2014-1175.ch005>
- French AD (2014) Idealized powder diffraction patterns for cellulose polymorphs. *Cellulose* 21:885–896
- Gedler G, Antunes M, Realinho V, Velasco JI (2012) Thermal stability of polycarbonate-graphene nanocomposite foams. *Polym Degrad Stab* 97:1297–1304. <https://doi.org/10.1016/j.polymdegradstab.2012.05.027>
- Gordobil O, Egués I, Urruzola I, Labidi J (2014) Xylan-cellulose films: improvement of hydrophobicity, thermal and mechanical properties. *Carbohydr Polym* 112:56–62. <https://doi.org/10.1016/j.carbpol.2014.05.060>
- Henriksson M, Henriksson G, Berglund LA, Lindström T (2007) An environmentally friendly method for enzyme-assisted preparation of microfibrillated cellulose (MFC) nanofibers. *Eur Polym J* 43:3434–3441. <https://doi.org/10.1016/j.eurpolymj.2007.05.038>
- Jacquet N et al (2011) Influence of steam explosion on the thermal stability of cellulose fibres. *Polym Degrad Stab* 96:1582–1588. <https://doi.org/10.1016/j.polymdegradstab.2011.05.021>
- Jiang F, Hsieh Y-L (2013) Chemically and mechanically isolated nanocellulose and their self-assembled structures. *Carbohydr Polym* 95:32–40. <https://doi.org/10.1016/j.carbpol.2013.02.022>
- Khouri S (2010) Experimental characterization and theoretical calculations of responsive polymeric systems. *UWSpace*
- Kumar V, Yang T (2002) HNO₃/H₃PO₄-NANO₂ mediated oxidation of cellulose—preparation and characterization of bioabsorbable oxidized celluloses in high yields and with different levels of oxidation. *Carbohydr Polym* 48:403–412
- Li W, Yang Y, Sha J, Zhou J, Qin C, Wang S (2018) The influence of mechanical refining treatments on the rheosedimentation properties of bleached softwood pulp suspensions. *Cellulose* 25:3609–3618
- Lin X, Wu Z, Zhang C, Liu S, Nie S (2018) Enzymatic pulping of lignocellulosic biomass. *Ind Crops Prod* 120:16–24. <https://doi.org/10.1016/j.indcrop.2018.04.033>
- Liu P, Guo X, Nan F, Duan Y, Zhang J (2017a) Modifying mechanical, optical properties and thermal processability of iridescent cellulose nanocrystal films using ionic liquid. *ACS Appl Mater Interfaces* 9:3085–3092. <https://doi.org/10.1021/acsami.6b12953>
- Liu Y, Lu P, Xiao H, Heydarifard S, Wang S (2017b) Novel aqueous spongy foams made of three-dimensionally dispersed wood-fiber: entrapment and stabilization with NFC/MFC within capillary foams. *Cellulose* 24:241–251. <https://doi.org/10.1007/s10570-016-1103-y>
- Long L, Tian D, Hu J, Wang F, Saddler J (2017) A xylanase-aided enzymatic pretreatment facilitates cellulose nanofibrillation. *Biores Technol* 243:898
- Lu P, Hsieh Y-L (2010) Preparation and properties of cellulose nanocrystals: rods, spheres, and network. *Carbohydr Polym* 82:329–336. <https://doi.org/10.1016/j.carbpol.2010.04.073>
- Martínez-Sanz M, López-Rubio A, Lagaron JM (2011) Optimization of the nanofabrication by acid hydrolysis of bacterial cellulose nanowhiskers. *Carbohydr Polym* 85:228–236. <https://doi.org/10.1016/j.carbpol.2011.02.021>
- Meng Q, Li H, Fu S, Lucia LA (2014) The non-trivial role of native xylans on the preparation of TEMPO-oxidized cellulose nanofibrils. *React Funct Polym* 85:142–150. <https://doi.org/10.1016/j.reactfunctpolym.2014.07.021>
- Meng Q, Fu S, Lucia LA (2016) The role of heteropolysaccharides in developing oxidized cellulose nanofibrils. *Carbohydr Polym* 144:187–195. <https://doi.org/10.1016/j.carbpol.2016.02.058>
- Milosavljevic I, Vahur Oja A, Suuberg EM (1996) Thermal effects in cellulose pyrolysis: relationship to char formation processes. *Ind Eng Chem Res* 35:653–662
- Nair SS, Yan N (2015) Effect of high residual lignin on the thermal stability of nanofibrils and its enhanced mechanical performance in aqueous environments. *Cellulose* 22:3137–3150. <https://doi.org/10.1007/s10570-015-0737-5>
- Nie S et al (2014) Kinetics study of oxidation of the lignin model compounds by chlorine dioxide. *Chem Eng J* 241:410–417. <https://doi.org/10.1016/j.cej.2013.10.068>
- Nie S, Wang S, Qin C, Yao S, Ebonka JF, Song X, Li K (2015) Removal of hexenuronic acid by xylanase to reduce adsorbable organic halides formation in chlorine dioxide bleaching of bagasse pulp. *Biores Technol* 196:413–417. <https://doi.org/10.1016/j.biortech.2015.07.115>
- Nie S, Zhang K, Lin X, Yan D, Liang H, Wang S (2018) Enzymatic pretreatment for the improvements of dispersion and film properties of cellulose nanofibrils. *Carbohydr Polym* 181:1136–1142. <https://doi.org/10.1016/j.carbpol.2017.11.020>
- Nishiyama Y, Sugiyama J, Chanzy H, Langan P (2003) Crystal structure and hydrogen bonding system in cellulose I α from synchrotron X-ray and neutron fiber diffraction. *J Am Chem Soc* 125:14300–14306. <https://doi.org/10.1021/ja037055w>
- Peng X, Ren J, Zhong L, Sun R (2011) Nanocomposite films based on xylan-rich hemicelluloses and cellulose nanofibers with enhanced mechanical properties. *Biomacromolecules* 12:3321–3329. <https://doi.org/10.1021/bm2008795>

- Peng Y, Gardner DJ, Han Y, Kiziltas A, Cai Z, Tshabalala MA (2013) Influence of drying method on the material properties of nanocellulose I: thermostability and crystallinity. *Cellulose* 20:2379–2392. <https://doi.org/10.1007/s10570-013-0019-z>
- Quiévy N, Jacquet N, Sclavons M, Deroanne C, Paquot M, Devaux J (2010) Influence of homogenization and drying on the thermal stability of microfibrillated cellulose. *Polym Degrad Stab* 95:306–314. <https://doi.org/10.1016/j.polymdegradstab.2009.11.020>
- Segal L, Creely J, Martin AJ, Conrad C (1959) An empirical method for estimating the degree of crystallinity of native cellulose using the X-ray diffractometer. *Text Res J* 29:786–794
- Shafizadeh F (1982) Introduction to pyrolysis of biomass. *J Anal Appl Pyrol* 3:283–305
- Shen DK, Gu S (2009) The mechanism for thermal decomposition of cellulose and its main products. *Biores Technol* 100:6496–6504. <https://doi.org/10.1016/j.biortech.2009.06.095>
- Song X, Jiang Y, Rong X, Wei W, Wang S, Nie S (2016) Surface characterization and chemical analysis of bamboo substrates pretreated by alkali hydrogen peroxide. *Biores Technol* 216:1098–1101. <https://doi.org/10.1016/j.biortech.2016.06.026>
- Stamm AJ (1956) Thermal degradation of wood and cellulose. *Ind Eng Chem Ind Eng Chem* 48:413–417
- Valkenburg MEV, Vaughn RL, Williams M, Wilkes JS (2005) Thermochemistry of ionic liquid heat-transfer fluids. *Thermochim Acta* 425:181–188
- Xu C, Cao L, Huang X, Chen Y, Lin B, Fu L (2017) Self-healing natural rubber with tailorable mechanical properties based on ionic supramolecular hybrid network. *ACS Appl Mater Interfaces* 9:29363–29373
- Yao S, Nie S, Yuan Y, Wang S, Qin C (2015) Efficient extraction of bagasse hemicelluloses and characterization of solid remainder. *Biores Technol* 185:21–27. <https://doi.org/10.1016/j.biortech.2015.02.052>
- Yao S, Nie S, Zhu H, Wang S, Song X, Qin C (2017) Extraction of hemicellulose by hot water to reduce adsorbable organic halogen formation in chlorine dioxide bleaching of bagasse pulp. *Ind Crops Prod* 96:178–185. <https://doi.org/10.1016/j.indcrop.2016.11.046>
- Zhu G, Zhu X, Xiao Z, Yi F (2012) Study of cellulose pyrolysis using an in situ visualization technique and thermogravimetric analyzer. *J Anal Appl Pyrol* 94:126–130
- Zhu H et al (2016) Wood-derived materials for green electronics, biological devices, and energy applications. *Chem Rev* 116:9305–9374. <https://doi.org/10.1021/acs.chemrev.6b00225>